# Core structures and mobility of ⟨c⟩ dislocations in magnesium

**Article** *in* Scripta Materialia · July 2017

DOI: 10.1016/j.scriptamat.2017.03.012



**6 authors**, including:

Haidong Fan
Sichuan University
**22** PUBLICATIONS **193** CITATIONS
SEE PROFILE

Qingyuan Wang
Sichuan University
**328** PUBLICATIONS **1,862** CITATIONS
SEE PROFILE

Xiaobao Tian
Sichuan University
**15** PUBLICATIONS **33** CITATIONS
SEE PROFILE

Jaafar A. El-Awady
Johns Hopkins University
**58** PUBLICATIONS **743** CITATIONS
SEE PROFILE

Scripta Materialia 135 (2017) 37–40

Contents lists available at ScienceDirect

Scripta Materialia

journal homepage: www.elsevier.com/locate/scriptamat

Regular Article

# Core structures and mobility of ⟨c⟩ dislocations in magnesium

Haidong Fan [a], Jing Tang [a], Xiaofeng Tian [b], Qingyuan Wang [a], Xiaobao Tian [a,*], Jaafar A. El-Awady [c]

[a] Key Laboratory of Energy Engineering Safety and Disaster Mechanics (Ministry of Education), Department of Mechanics, Sichuan University, Chengdu 610065, China
[b] The College of Nuclear Technology and Automation Engineering, Chengdu University of Technology, Chengdu 610059, China
[c] Department of Mechanical Engineering, Whiting School of Engineering, The Johns Hopkins University, Baltimore, MD 21218, USA

ARTICLE INFO

*Article history:*
Received 28 December 2016
Received in revised form 28 February 2017
Accepted 9 March 2017
Available online 27 March 2017

*Keywords:*
Magnesium
⟨c⟩ dislocations
Molecular dynamics
Density functional theory

ABSTRACT

The core structures and mobility of ⟨c⟩ dislocations in magnesium were predicted using both density functional theory and molecular dynamics simulations. The pure edge and screw cores are compact at 0 K. With increasing temperature up to 700 K, the edge dislocation dissociates into two ⟨c⟩/2 partials on the basal plane, but remains immobile. The screw dislocation remains compact and continuously cross-slips between the three prismatic planes. At room temperature, the screw dislocation only glides after emitting a vacancy at 420 MPa. The Peierls stress of the dislocation after vacancy emission is 50 MPa.



Magnesium (Mg) is the lightest-weight structural metal. However, its poor ductility seriously limits its applications in many industries. Based on the hexagonal closed packed (HCP) lattice structure of Mg, dislocations can be classified to be ⟨a⟩, ⟨c⟩ or ⟨c + a⟩ dislocation according to their Burgers vectors. Enhancing the ductility of Mg depends greatly on the non-basal deformation modes required to accommodate c-axis deformation, including ⟨c + a ⟩ and ⟨c⟩ dislocations. Among the three types of dislocations, ⟨a ⟩ and ⟨c + a⟩ dislocations have received ample attentions in recent years. However, so far, the fundamental understanding of ⟨c⟩ dislocations, including the dislocation core structure, mobility, and cross-slip, remains elusive. It is still questioned whether ⟨c⟩ dislocation can contribute to plastic slip or not. Recently it has been shown that ⟨c + a⟩ dislocations can decompose into ⟨a⟩ and ⟨c⟩ dislocations on the basal planes [1–4]. Since this decomposition of ⟨c + a⟩ dislocations can adversely affect the slip contribution of ⟨c + a⟩ dislocations, it is of great importance to develop a quantified understanding of ⟨c⟩ dislocations. This is also significant for incorporating ⟨c⟩ dislocation plasticity in micro-scale simulations, such as discrete dislocation dynamics and crystal plasticity simulations [5–8].

In the current study, the core structures and mobility of ⟨c⟩ dislocations are studied using density functional theory (DFT), molecular statics (MS), and molecular dynamics (MD) simulations. The DFT calculations have been performed by the ab-initio total-energy and molecular-dynamics program VASP (Vienna ab-initio simulation program) [9,10], using exchange correlation function parameterization within the generalized gradient approximation [11]. Plane waves with a kinetic energy up to 130 eV were used to expand the wave functions, and the electronic charge density was obtained by a $5 \times 1 \times 1$ k-point grid within the Brillouin zone. The simulation cell size is $0.64 \times 6.8 \times 12.2$ nm$^3$, containing 2390 atoms, for the edge dislocation simulations, and $0.52 \times 6.4 \times 12.2$ nm$^3$, containing 1760 atoms, for the screw dislocation simulations. Periodic boundary conditions are imposed along all three directions, therefore two opposite-signed ⟨c⟩ dislocations that are 6 nm vertically apart were introduced into the simulation cell by initializing all atoms according to the Volterra fields. Structural optimization was performed until the force acting on each atom is below a threshold of 0.01 eV/Å. Besides, the generalized stacking fault energy (GSFE) curve along ⟨c⟩ direction on prismatic plane was calculated on a simulation cell $0.52 \times 0.64 \times 13.8$ nm$^3$. All the atoms shown in this work are colored by common neighbor analysis (CNA) as indicated by the legend in Fig. 1, and all images are exported using the visualization tool OVITO [12].

The edge and screw ⟨c⟩ dislocation cores as predicted from DFT calculations are shown in Fig. 1. The edge dislocation core is compact and resides along the intersection line between the basal and prismatic planes. In Fig. 1(b) the positive and negative screw dislocation cores are shown, both of which are also compact. Although the screw dislocation cores were initialized on horizontal prismatic planes, after relaxation both reside on 60° prismatic planes. This is because screw dislocations can easily cross slip between the different prismatic planes. Furthermore, the screw dislocations were observed to glide during the minimization process, as shown in Fig. 1(b1)–(b4). In Fig. 1(b1), the upper screw dislocation starts gliding downwards along the 60° prismatic plane after emitting a vacancy, while the lower dislocation does not move. The upper dislocation then cross slips onto the −60° prismatic plane, and continues to glide towards the lower dislocation. Finally,

* Corresponding author.
*E-mail address:* xbtian@scu.edu.cn (X. Tian).

http://dx.doi.org/10.1016/j.scriptamat.2017.03.012
1359-6462/

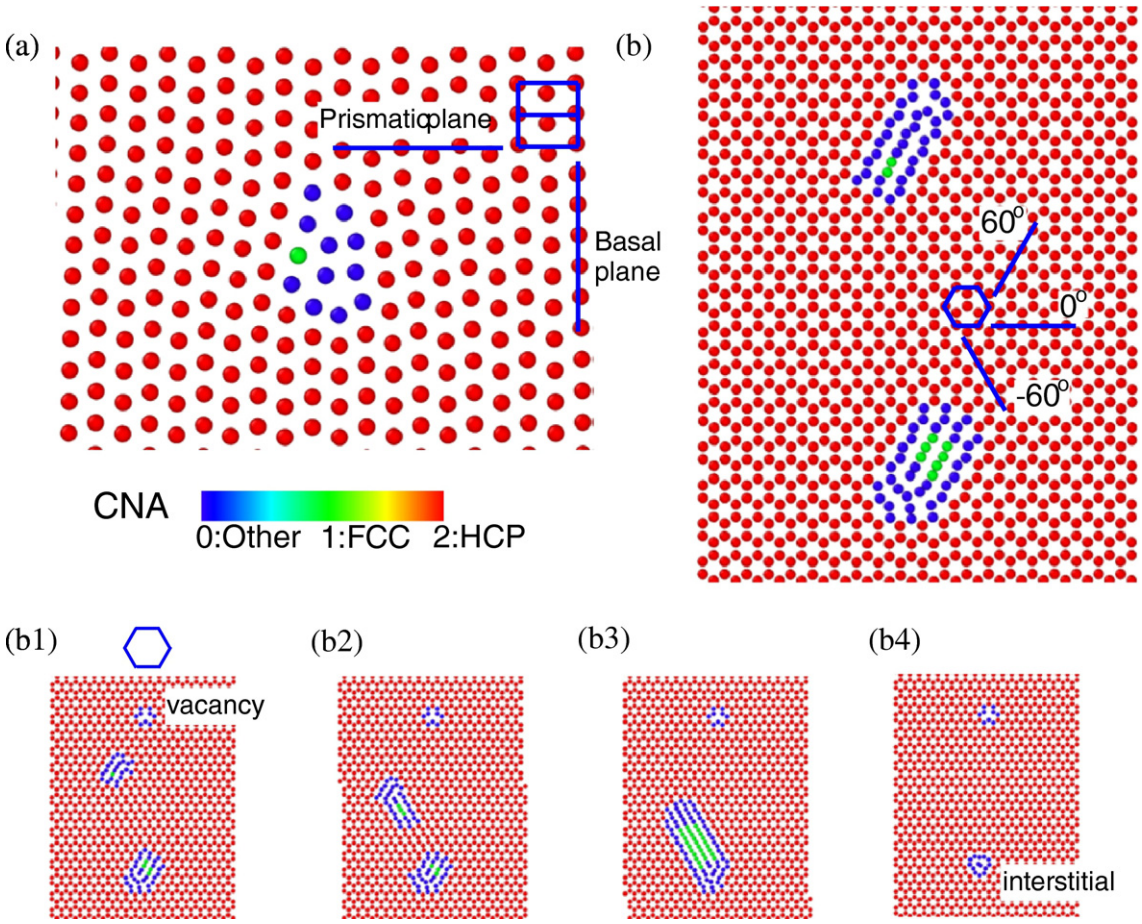


**Fig. 1.** The core structures of (a) edge and (b) screw ⟨c⟩ dislocations as predicted from DFT calculations. The sequence (b1) through (b4) shows the glide, cross-slip and annihilation of the screw dislocation cores.

these two opposite-signed dislocations annihilate fully and an interstitial is left behind. As will be shown in the following MD simulations, a stress driven vacancy emission is always observed from the screw dislocation core before steady glide is attained. In the DFT calculations, it is clear that this vacancy emission does not occur simultaneously for both screw dislocations. As such, the upper screw dislocation emits a vacancy and glides while the bottom dislocation remains immobile for the duration of the simulation.

It should be noted that the current DFT calculation only predicts the dislocation cores at 0 K. In addition, the simulation cell is very small, thus, the local stress is not zero due to the dislocation interactions and boundary conditions. Despite this, the DFT predictions can be treated as a reference state of the dislocation cores. In order to calculate the dislocation mobility and temperature effects, both MS and MD simulations are employed, which facilitate a large scale simulation. These simulations were conducted using the open source code LAMMPS [13]. Only one dislocation core is introduced into the center of simulation cells having dimensions of $30 \times 30 \times 0.64$ or $30 \times 30 \times 0.52$ nm$^3$, with the dislocation line being parallel to the shortest dimension. Periodic boundary conditions are imposed along the dislocation line and glide directions, while free boundary conditions are imposed along the third direction. An energy minimization step is then performed, which leads to an initial dislocation core under stress-free condition. The temperature of the simulation cell is increased using the NPT ensemble by maintaining a zero pressure state and a heating rate of 1.0 K/ps, until the target temperature, $T$, is reached [14]. A pure shear stress along the dislocation Burgers vector is finally imposed on the top and bottom surfaces using the NVE ensemble to study the dislocation mobility [15]. The pure shear stress increases linearly with simulation time. In order to avoid inertia effects introduced by a high loading rate [16], a low stress rate of 0.77 MPa/ps is employed. In addition, the dislocation core energy per unit length $E_c$ was calculated from the energy increase within a cylindrical region of radius 5 nm around the dislocation core. The GSFE curve along ⟨c⟩ direction on prismatic plane was calculated on a simulation cell $15 \times 15 \times 15$ nm$^3$.

Three commonly used Mg potentials were adopted and compared with the DFT observations. The potentials used are the modified embedded atom method (MEAM) potential developed by Kim et al. [17] and the EAM potentials developed by Sun et al. [18] and Liu et al. [19]. The dislocation cores after minimization (0 K and 0 MPa) predicted from MS simulations are shown in Fig. 2. The edge dislocation core predicted from the Kim et al. potential [17] is compact and in good agreement with the one predicted from the DFT calculations. However, the other two potentials predict strange core structures, obviously at odds with the DFT calculations. On the other hand, the screw dislocation cores predicted by the three potentials are similar, and all reside on a prismatic plane. Although the screw dislocation cores from the MS simulations are similar to the DFT in shape, they are more compact because they are in a stress-free condition. In addition, the core energy of the screw dislocation is lower than that of edge dislocation. The GSFE curves as predicted by the three potentials and DFT are shown in Fig. 2(c). The curve of DFT is lower than those of the three potentials, which agrees with the previous comparisons of the ⟨c + a⟩ GSFE curves [20]. The curves of Kim potential and DFT display no local minima during the displacement, which are corresponding with the observation that the edge dislocation core is compact with no stacking faults. The other two potentials predict (quasi) local minima, and the dislocation cores have stacking faults residing on two prismatic planes. This is probably why

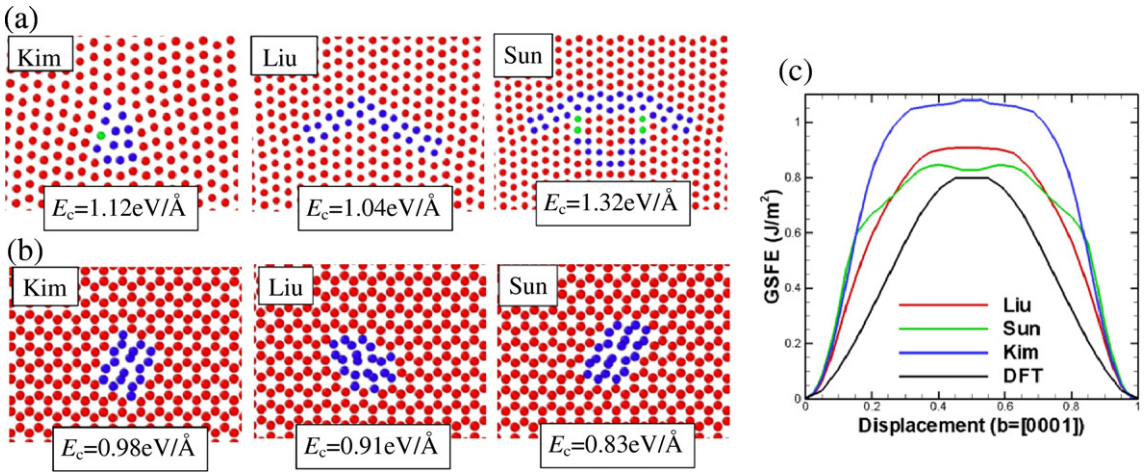


**Fig. 2.** The core structures of (a) edge and (b) screw ⟨c⟩ dislocations and (c) the GSFE curves as predicted from Kim, Liu and Sun potentials and DFT.

the Kim potential predicts dislocation cores that are in good agreement with DFT versus the other two potentials. Together with the previous comparisons of the three potentials for ⟨c + a⟩ dislocations [20], it can be concluded that the Kim et al. potential [17] predicts the ⟨c⟩ and ⟨c + a⟩ dislocation cores more accurately, as compared to the DFT calculations, than the two EAM potentials.

The effect of temperature on the edge and screw ⟨c⟩ dislocation cores is shown in Fig. 3 for 0 K, 300 K, 500 K, and 700 K. To facilitate visualization, thermal fluctuations are removed by performing conjugate gradient relaxation for 50 steps. It is clear that the screw dislocation cores display weak temperature dependence. With increasing temperature from 0 K to 700 K, the screw core width increases, but consistently remains on the prismatic plane, retaining a compact structure without any dissociation. On the other hand, the edge dislocation cores show a strong dependence on temperature. The edge core at 0 K is compact, but becomes dissociated with increasing temperatures. The stacking faults (SFs) connecting the two partials also increase in width as the temperature increases. According to the HCP crystalline structure, the ⟨c⟩ dislocation is expected to dissociate on the prismatic plane. Surprisingly, the dissociated dislocation cores predicted from the current simulations reside on the basal plane. According to the Burgers circuit analysis, shown in Fig. 3(a) at 700 K, the full ⟨c⟩ dislocation dissociates into two ⟨c⟩/2 partials, as follows

$$c \rightarrow c/2 + SF_{basal} + c/2 \quad (1)$$

Furthermore, the mobility of the edge and screw ⟨c⟩ dislocations under a pure shear stress was also investigated. The edge dislocation is observed to be immobile up to a shear stress larger than 500 MPa at all considered temperatures. This can be attributed to the dissociation of the edge ⟨c⟩ dislocations on the basal plane. On the other hand, the dislocation velocity versus applied shear stress curve for the screw dislocation at 300 K is shown in Fig. 4. The dislocation glide process is also shown in the online Supplementary movie. Below a shear stress of 420 MPa, the screw dislocation does not glide; however, the dislocation core continually changes its slip plane by cross-slip along the three prismatic planes, or resides on three prismatic planes simultaneously. At a stress of 420 MPa, the dislocation begins to glide stably on the horizontal prismatic plane (i.e. plane with the maximum resolved shear stress) after emitting a vacancy behind, as shown in the online Supplementary movie and the inset in Fig. 4. The vacancy emission is in agreement with the DFT observations discussed above. It can be seen the screw ⟨c⟩ dislocation is glissile with a high critical gliding stress of 420 MPa. It is worth noting that this glide process is also observed at other temperatures, but with a critical gliding stress that decreases with increasing temperature, namely 460 MPa at 100 K, 420 MPa at 300 K, 340 MPa at 500 K, and 380 MPa at 700 K. The current simulations were performed in a simulation cell with small size along the dislocation line, and thus only one vacancy was emitted. Simulations with a much longer dislocation show that many vacancies are emitted randomly on the dislocation slip plane since they are not emitted synchronously.

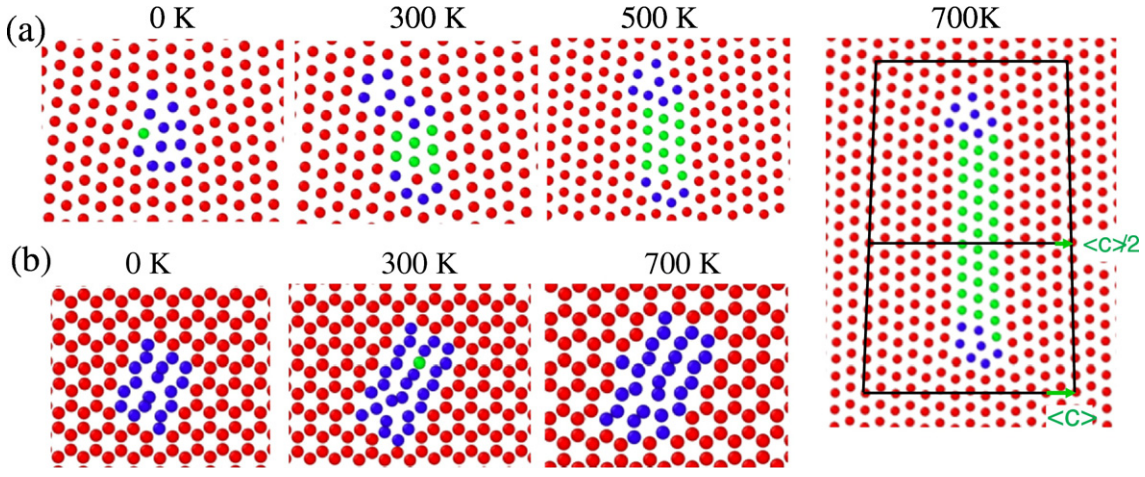


**Fig. 3.** The effect of temperature on the core structures of (a) edge and (b) screw ⟨c⟩ dislocations as predicted by the Kim potential.

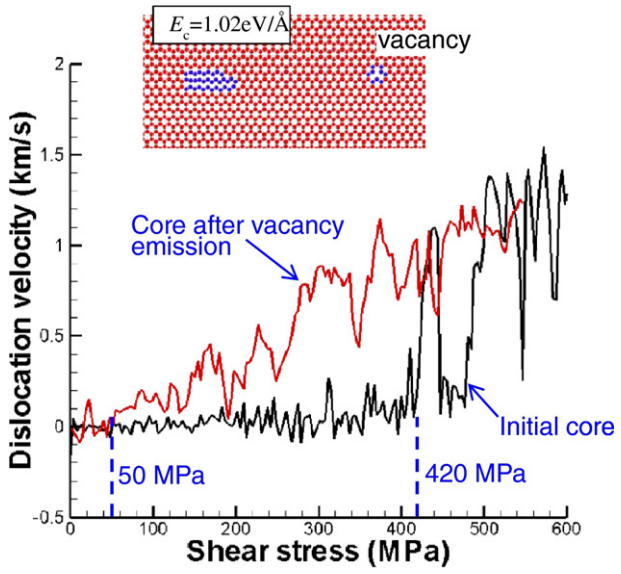


**Fig. 4.** Mobility curves at 300 K for the initial screw dislocation core and the core after vacancy emission.

The mobility of the screw dislocation depends strongly on the vacancy emission. Although vacancy emission was commonly observed in previous MD simulations on the ⟨c + a⟩ dislocations in magnesium due to the formation of dislocation jogs [3,21], the current vacancy formation is not a result of the dislocation jogs, since the dimension along the dislocation is only a periodic lattice. From the energy increase after vacancy emission (inset of Fig. 4), it is observed that the dislocation core energy after vacancy emission is slightly higher than the initial core energy. This indicates that the initial dislocation core structure is an energetically favorable structure, while the vacancy emission is driven by stress and temperature. This also suggests that the vacancy emission could be attributed to a core structure correction to make it glissile.

To investigate the screw dislocation after the vacancy emission, the simulation cell was unloaded following the vacancy emission and then reloaded. The mobility curve for this dislocation core is also shown in Fig. 4. In this case the dislocation core is observed to first cross-slip continually between the three prismatic planes, until the stress reaches a critical stress of ~50 MPa at which the dislocation core begins to glide stably on the horizontal prismatic plane without any vacancy emission.

Although the ⟨c⟩ dislocations received rare attentions, they are significant for the property of ⟨c + a⟩ dislocations. In previous studies [2–4], the pyramidal ⟨c + a⟩ dislocations were observed to decompose into edge ⟨a⟩ and edge ⟨c⟩ dislocations, both of which reside on the basal plane. The ⟨a⟩ and ⟨c⟩ dislocations then combine and form a⟨c + a⟩ dislocation dissociated on the basal plane, which thus limits the contribution of edge ⟨c + a⟩ dislocations to plasticity in Mg. Based on the current analysis of the ⟨c⟩ dislocations it can be suggested that the thermally activated dissociation of edge ⟨c + a⟩ dislocations on the basal plane is mostly driven by the thermally activated dissociation of the ⟨c⟩ component of the dislocation on the basal planes. This suggests that the ⟨c + a⟩ dislocation behavior is controlled predominantly by its ⟨c⟩ component.

The ductility enhancement of Mg depends greatly on the non-basal deformation modes accommodating c-axis deformation including ⟨c ⟩ and ⟨c + a⟩ dislocations. The present work showed that the Peierls stress of the ⟨c⟩ screw dislocation is ~50 MPa possibly, which would be an alternative method to accommodate the c-axis deformation. As shown by Agnew et al. [1,22], dense dislocations having ⟨c⟩ component (⟨c⟩ and ⟨c + a⟩) were observed in the Mg-Li alloys having good ductility. Therefore, future efforts can be made towards regulating the ⟨c⟩ dislocations, such as decreasing the Peierls stress, and/or preventing the edge dislocation from dissociating on the basal planes.

In summary, the ⟨c⟩ dislocation core structures were calculated using the density functional theory. The dislocation mobility and effect of temperature were also investigated by molecular dynamics simulations. The edge dislocation cores were observed to be sessile due to their dissociation on the basal planes, while the screw dislocations are compact and immobile before emitting a vacancy at 420 MPa at room temperature. After vacancy emission, the dislocation core is highly glissile and the Peierls stress is ~50 MPa. The ⟨c⟩ dislocation could be regulated to accommodate the c-axis deformation and produce an enhanced ductility.

Supplementary data to this article can be found online at http://dx.doi.org/10.1016/j.scriptamat.2017.03.012.

## Acknowledgements

The financial support from the Natural Science Foundation of China (11672193, 11602154) and Program for Innovative Research Team (IRT14R37) is acknowledged. Author JAE acknowledges support by the US Army Research Laboratory (#W911NF-12-2-0022) and by the National Science Foundation (#DMR-1609533).

## References

[1] S.R. Agnew, J.A. Horton, M.H. Yoo, Metall. Mater. Trans. A 33 (2002) 851–858.
[2] Z. Wu, W.A. Curtin, Nature 526 (2015) 62–67.
[3] H. Fan, Q. Wang, X. Tian, J.A. El-Awady, Scr. Mater. 127 (2017) 68–71.
[4] Y. Tang, J.A. El-Awady, Mater. Sci. Eng. A 618 (2014) 424–432.
[5] J. Zhang, S.P. Joshi, J. Mech. Phys. Solids 60 (2012) 945–972.
[6] H. Fan, S. Aubry, A. Arsenlis, J.A. El-Awady, Acta Mater. 92 (2015) 126–139.
[7] S. Aubry, M. Rhee, G. Hommes, V.V. Bulatov, A. Arsenlis, J. Mech. Phys. Solids 94 (2016) 105–126.
[8] H. Minsheng, L. Shuang, L. Zhenhuan, Model. Simul. Mater. Sci. Eng. 25 (2017) 035001.
[9] G. Kresse, J. Furthmüller, Phys. Rev. B 54 (1996) 11169–11186.
[10] G. Kresse, J. Hafner, Phys. Rev. B 47 (1993) 558–561.
[11] J.P. Perdew, K. Burke, M. Ernzerhof, Phys. Rev. Lett. 77 (1996) 3865–3868.
[12] A. Stukowski, Model. Simul. Mater. Sci. Eng. 18 (2010) 015012.
[13] S. Plimpton, J. Comput. Phys. 117 (1995) 1–19.
[14] Y. Zhu, Z. Li, M. Huang, Y. Liu, Int. J. Plast. 72 (2015) 168–184.
[15] H. Fan, J.A. El-Awady, Mater. Sci. Eng. A 644 (2015) 318–324.
[16] H. Fan, J.A. El-Awady, Q. Wang, J. Nucl. Mater. 458 (2015) 176–186.
[17] K.-H. Kim, J.B. Jeon, B.-J. Lee, Calphad 48 (2015) 27–34.
[18] D.Y. Sun, M.I. Mendelev, C.A. Becker, K. Kudin, T. Haxhimali, M. Asta, J.J. Hoyt, A. Karma, D.J. Srolovitz, Phys. Rev. B 73 (2006) 024116.
[19] X.-Y. Liu, J.B. Adams, F. Ercolessi, J.A. Moriarty, Model. Simul. Mater. Sci. Eng. 4 (1996) 293–303.
[20] M. Ghazisaeidi, L.G. Hector Jr., W.A. Curtin, Scr. Mater. 75 (2014) 42–45.
[21] Y. Tang, J.A. El-Awady, Acta Mater. 71 (2014) 319–332.
[22] S.R. Agnew, M.H. Yoo, C.N. Tomé, Acta Mater. 49 (2001) 4277–4289.